Neuropilin-1 functions as a VEGFR2 co-receptor to guide developmental angiogenesis independent of ligand binding

Maria V Gelfand, Nellwyn Hagan, Aleksandra Tata, Won-Jong Oh, Baptiste Lacoste, Kyu-Tae Kang, Justyna Kopycinska, Joyce Bischoff, Jia-Huai Wang, Chenghua Gu

DOI: http://dx.doi.org/10.7554/eLife.03720

Cite as: eLife 2014;10.7554/eLife.03720

Received: 18 June 2014
Accepted: 20 September 2014
Published: 22 September 2014

Neuropilin-1 functions as a VEGFR2 co-receptor to guide developmental angiogenesis independent of ligand binding.

Maria V. Gelfand[1*], Nellwyn Hagan[1*], Aleksandra Tata[1*], Won-Jong Oh[1,2], Baptiste Lacoste[1], Kyu-Tae Kang[3,4], Justyna Kopycinska[1], Joyce Bischoff[3], Jia-huai Wang[5], Chenghua Gu[1,6]

[1] Department of Neurobiology, Harvard Medical School, 220 Longwood Ave., Boston, MA 02115, U.S.A.
[2] Korea Brain Research Institute, Daegu, Republic of Korea
[3] Vascular Biology Program and Department of Surgery, Boston Children's Hospital, Harvard Medical School, Boston, MA, USA
[4] College of Pharmacy, Duksung Women's University, Seoul, Republic of Korea
[5] Dana-Farber Cancer Institute, 450 Brookline Ave., Boston, MA 02215, U.S.A.

*authors contributed equally to this work

[6] Correspondence and requests for materials should be addressed to C.G.

Chenghua Gu (chenghua_gu@hms.harvard.edu)
Department of Neurobiology, Harvard Medical School
220 Longwood Ave.
Boston, MA 02115, U.S.A.
(Ph) 617-432-6364 (Fax) 617-432-1639

Completing Interests Statement

The authors declare that no completing interests exist.

Abstract

During development, tissue repair, and tumor growth, most blood vessel networks are generated through angiogenesis. Vascular endothelial growth factor (VEGF) is a key regulator of this process and currently, both VEGF and its receptors, VEGFR1, VEGFR2, and Neuropilin1 (NRP1), are targeted in therapeutic strategies for vascular disease and cancer. NRP1 is essential for vascular morphogenesis, but how NRP1 functions to guide vascular development has not been completely elucidated. Here, we generated a mouse line harboring a point mutation in the endogenous Nrp1 locus that selectively abolishes VEGF-NRP1 binding ($Nrp1^{VEGF-}$). $Nrp1^{VEGF-}$ mutants survive to adulthood with normal vasculature revealing that NRP1 functions independent of VEGF-NRP1 binding during developmental angiogenesis. Moreover, we found that *Nrp1*-deficient vessels have reduced VEGFR2 surface expression *in vivo* demonstrating that NRP1 regulates its co-receptor, VEGFR2. Given the resources invested in NRP1 targeted anti-angiogenesis therapies, our results will be integral for developing strategies to re-build vasculature in disease.

Introduction

Blood vessels provide oxygen and nutrients to cells throughout the body and are essential for tissue homeostasis and repair as well as tumor growth. The molecular mechanisms underlying angiogenesis have become increasingly clear and VEGF is an essential player in this process (Carmeliet et al., 1996, 1999; Chung and Ferrara, 2011; Coultas et al., 2005; Ferrara et al., 1996, 2003; Iruela-Arispe and Dvorak, 1997; Maes et al., 2004; Miquerol et al., 1999; Olsson et al., 2006; Rossant and Hirashima, 2003; Ruhrberg et al., 2002; Stalmans et al., 2002). VEGF operates by interacting with three receptors, VEGFR1, VEGFR2 (KDR/Flk1), and NRP1 (Chung

and Ferrara, 2011; Ferrara et al., 2003). Although these three receptors are expressed in spatially and temporally overlapping patterns, they are thought to play different roles in VEGF signaling. The main receptor for VEGF, VEGFR2, is a receptor tyrosine kinase whose activity is crucial for VEGF signaling (Olsson et al., 2006). Upon binding VEGF, VEGFR2 phosphorylates intracellular targets leading to a multitude of cellular responses including proliferation, migration, and transcriptional modification via signaling pathways such as PI3K, Src, and PLCϒ (Olsson et al., 2006). In contrast, NRP1 is a multifaceted transmembrane receptor that not only binds VEGF and forms a complex with VEGFR2 but also binds a structurally and functionally unrelated family of traditional axon guidance cues, the secreted class 3 semaphorins (SEMA3) (He and Tessier-Lavigne, 1997; Kolodkin et al., 1997; Soker et al., 1998). Consistent with these binding partners, *Nrp1*$^{-/-}$ mice are embryonic lethal with both neural and vascular defects (Kawasaki et al., 1999; Kitsukawa et al., 1997), indicating that NRP1 protein is instrumental for developmental angiogenesis. However, how NRP1 functions in conjunction with multiple ligands and receptors to guide vascular development remains elusive.

Previous work has started to systematically dissect NRP1 function *in vivo* using a combination of structure-function analyses and mouse genetic approaches. In particular, endothelial-specific NRP1 knock-outs (*Tie2-Cre;Nrp1*$^{fl/-}$) recapitulate the devastating vascular defects observed in *Nrp1*$^{-/-}$ mice - the vascular network is poorly developed and large endothelial cell aggregates form within the brain (Gu et al., 2003). This result strongly demonstrates that NRP1 is cell autonomously required in endothelial cells for its absolutely essential function in developmental angiogenesis. To pinpoint how SEMA3-NRP1 versus VEGF-NRP1 binding contribute to NRP1's critical role in vascular development, previous work generated a knock-in mouse line,

84 *Nrp1*$^{Sema-}$, in which SEMA3-NRP1 interactions were abolished and VEGF-NRP1 binding was
85 maintained (Gu et al., 2003). *Nrp1*$^{Sema-}$ mice mimicked the neural defects observed in the *Nrp1*$^{-/-}$
86 but did not exhibit any vascular abnormalities. These data suggest that SEMA3-NRP1 binding
87 does not mediate NRP1's important function in vascular morphogenesis and point to the
88 hypothesis that instead VEGF-NRP1 interactions may be integral for angiogenesis.
89
90 Currently, the dominant view in the field asserts that VEGF-NRP1 binding enhances VEGFR2
91 activity and downstream signaling. Yet, the functional consequence of VEGF-NRP1 interactions
92 has only been studied indirectly using *in vitro* methodology and blocking antibodies *in vivo*
93 (Herzog et al., 2011; Pan et al., 2007). Specifically, an antibody inhibiting VEGF-NRP1 binding
94 was found to interfere with retinal vascular remodeling as well as tumor angiogenesis (Pan et al.,
95 2007) and is currently being developed as a therapeutic strategy to block vessel outgrowth. This
96 study suggests that VEGF-NRP1 binding facilitates pathological angiogenesis. However, *in vivo*
97 evidence describing a role for VEGF-NRP1 binding in vascular development is currently lacking
98 and the precise function of NRP1 in VEGF-mediated angiogenesis urgently needs to be
99 addressed.
100
101 To delineate the role of VEGF-NRP1 interactions, we identified a single amino acid residue in
102 the b1 domain of NRP1 that is necessary for VEGF-NRP1 binding and generated a mouse
103 harboring this point mutation to abolish VEGF-NRP1 interactions *in vivo* (*Nrp1*$^{VEGF-}$).
104 Surprisingly, although VEGF-NRP1 binding was successfully eliminated, *Nrp1*$^{VEGF-}$ mutants
105 survived into adulthood and did not display any of the severe vascular phenotypes seen in either
106 the *Nrp1*$^{-/-}$ or the endothelial-specific NRP1 knock-out. Upon closer examination, NRP1-

deficient blood vessels in the endothelial-specific NRP1 knock-out exhibited reduced VEGFR2 surface expression, a phenomenon not observed in the *Nrp1*$^{VEGF-}$ mutant. These results challenge the well-accepted view that NRP1 requires VEGF-NRP1 binding to facilitate developmental angiogenesis and points to a provocative new hypothesis that the angiogenic role of NRP1 lies in its capacity as a VEGFR2 co-receptor. Interestingly, retinal angiogenesis and blood flow recovery following hind limb ischemia were mildly perturbed in the *Nrp1*$^{VEGF-}$ mutant suggesting that the postnatal vascular system is uniquely sensitive to the loss of VEGF-NRP1 binding. Together, this work not only significantly advances our basic scientific understanding of how NRP1 functions in VEGF-mediated angiogenesis, but also provides new insights that may facilitate the development of more effective NRP1 targeted anti-angiogenesis therapies.

Results

Identification of a Nrp1 mutation that abolishes VEGF-NRP1 binding

We sought to elucidate the *in vivo* function of VEGF-NRP1 binding by generating a mouse line that selectively disrupts VEGF binding to NRP1. A previous structure-function analysis revealed that the b1 domain of NRP1 is necessary and sufficient for VEGF binding (Gu et al., 2002). However, this b1 region is also required for SEMA3-NRP1 interactions, so a series of *Nrp1* variants containing smaller deletions in the b1 domain were engineered with site-directed mutagenesis to identify a region specific for VEGF-NRP1 binding (Figure 1A). Based upon previous publications, we first targeted two specific sites in the b1 domain: the 7-residue binding site of the Pathologische Anatomie Leiden-Endothelium (PAL-E) monoclonal antibody which competes with VEGF for NRP1 binding (Jaalouk et al., 2007) and the 3-residue binding site of the VEGF analog tuftsin (Vander Kooi et al., 2007) (Figure 1A-B). COS-1 cells were transfected

with wild-type (WT) or mutant *Nrp1* constructs and assessed for NRP1 expression. PAL-E and tuftsin binding site mutations did not affect NRP1 protein expression at the cell surface as examined by non-permeabilized antibody staining (Figure 1C, Figure 1 – figure supplement 1). Ligand binding to NRP1 was assessed using alkaline phosphatase-tagged VEGF (AP-VEGF) and SEMA3A (AP-SEMA3A) in conjunction with alkaline phosphatase histochemistry. All of the PAL-E or tuftsin binding site variants were capable of abolishing VEGF-NRP1 binding, but unfortunately, also eliminated SEMA3-NRP1 binding (Figure 1C, Figure 1 – figure supplement 1).

We decided to use an unbiased approach and designed our subsequent *Nrp1* variants based upon the crystal structure of the full NRP1 b1 domain. Specifically, we identified a hydrophilic region comprised of several negatively charged residues that provided a promising mutagenesis site for abolishing of VEGF-NRP1 binding (Figure 1A). Several of these residues were mutated to amino acids of the opposite charge in order to preserve the hydrophilic nature of the region. As with previous *Nrp1* variants, NRP1 surface expression was unperturbed in transfected COS-1 cells (Figure 1C). One of these mutations (E282K) did not affect the binding of either AP-SEMA3A or AP-VEGF, while others (E282K and E420K) eradicated binding of both ligands (Figure 1 – figure supplement 1). However, the D320K mutation converting aspartic acid 320 into lysine ($Nrp1^{D320K}$) successfully abolished VEGF-NRP1 binding while conserving AP-SEMA3A binding as demonstrated through alkaline phosphatase histochemical staining on transfected COS-1 cells (Figure 1C, Figure 2A,C). Moreover, the $Nrp1^{D320K}$ mutation also abolished the binding of other VEGF family members including Placenta Growth Factor (PlGF) and Vascular Endothelial Growth Factor B (VEGFB) (Figure 2 – figure supplement 1). In a

liquid alkaline phosphatase activity assay, *Nrp1*^{D320K} was co-expressed with *PlexinA4* (*Plex4A*) to more accurately reflect the *in vivo* situation in which SEMA3A signals through a holoreceptor complex of both NRP1 and PlexinA. AP-SEMA3A binding levels to WT NRP1 and NRP1^{D320K} were indistinguishable (Figure 2D) and the dissociation constant (K_D) of SEMA3A-NRP1^{D320K}/PlexinA4 was unchanged from that of SEMA3A-NRP1/PlexinA4 further verifying that the SEMA3A-NRP1/PlexinA4 interaction was intact (Figure 2E). Finally, Western blot analysis confirmed that NRP1 protein expression levels were equivalent in COS-1 cells transfected with *WT Nrp1* and *Nrp1*^{D320K} (Figure 2B). Taken together, these data demonstrate that the *Nrp1*^{D320K} mutation is sufficient to eliminate VEGF binding and maintain SEMA3A binding *in vitro*.

Generation and validation of the Nrp1^{VEGF-} *mouse line*

A gene replacement strategy was implemented to generate a mouse line harboring the *Nrp1*^{D320K} mutation in the endogenous *Nrp1* locus, delineated as *Nrp1*$^{VEGF-}$. Specifically, two base pair mutations were introduced into exon 6 of the mouse *Nrp1* gene to produce the D320K mutation in the endogenous Asp320 location (Figure 3A). After recombineering, embryonic stem cells were screened via PCR and sequenced to confirm that the D320K mutation was appropriately introduced into the *Nrp1* locus (Figure 3 – figure supplement 1A-C). Once *Nrp1*$^{VEGF-}$ mice were obtained, the presence of the D320K mutation was verified by sequencing (Figure 3 – figure supplement 1D). Importantly, *Nrp1*$^{VEGF-}$ mutants expressed normal levels of NRP1 protein as assessed by Western blot on embryonic day 14.5 (E14.5) lung and adult heart, brain, lung and kidney (Figure 3C, Figure 3 – figure supplement 2D). AP-VEGF and AP-SEMA3A binding was examined at E12.5 in the dorsal root entry zone (DREZ), where NRP1-expressing axons from the

dorsal root ganglion enter the spinal cord. Both AP-VEGF and AP-SEMA3A bound to the DREZ in control animals (Figure 3B) while AP-VEGF binding to the DREZ was abolished in the *Nrp1*$^{VEGF-}$ mutant (Figure 3B), confirming that this mutation eliminated VEGF-NRP1 binding *in vivo*. Moreover, NRP1 immunostaining and AP-SEMA3A binding to the DREZ appeared similar between *Nrp1*$^{VEGF-}$ and control littermates (Figure 3B). Finally, *Nrp1*$^{VEGF-}$ mutants failed to display the perinatal lethality observed in *Nrp1*$^{Sema-}$ mutants (Gu et al., 2003), further confirming functional SEMA3-NRP1 binding in *Nrp1*$^{VEGF-}$ mice (Figure 3 – figure supplement 1).

VEGF-NRP1 binding is not required for developmental angiogenesis

Despite the embryonic lethality previously described in *Nrp1*$^{-/-}$ and *Tie2-Cre,Nrp1*$^{fl/-}$ animals, *Nrp1*$^{VEGF-}$ mice were born at expected Mendelian ratios and maintained their vitality into adulthood ($P>0.05$ for observed vs. expected, Figure 3 – figure supplement 2E). *Nrp1*$^{VEGF-}$ mutants exhibited normal gross morphology throughout embryonic and postnatal stages (Figure 3D,E) and failed to develop the cardiac defects previously observed in the *Nrp1*$^{-/-}$, *Tie2-Cre;Nrp1*$^{fl/-}$, and *Nrp1*$^{Sema-}$ mutants (Figure 3 – figure supplement 2A). Moreover, *Nrp1*$^{VEGF-}$ animals displayed normal body weight (Figure 3F), organ growth (Figure 3 – figure supplement 2B,C), and fertility.

To thoroughly examine vascular integrity during development, isolectin immunostaining was employed to visualize blood vessels in embryonic and perinatal brain sections and vessel ingression, morphology, and branching were assessed in the *Nrp1*$^{VEGF-}$ mutant. Surprisingly, *Nrp1*$^{VEGF-}$ animals did not exhibit any of the vascular abnormalities observed in the endothelial-

specific NRP1 knockout. As shown in Figure 4A and quantified in Figure 4B-C, cortical vessel ingression was nearly absent in *Tie2-Cre;Nrp1*$^{fl/fl}$ animals at E11.5 while ingression was unaffected in *Nrp1*$^{VEGF-}$ mutants. In addition, *Tie2-Cre;Nrp1*$^{fl/fl}$ animals had abnormally large vascular aggregates distributed throughout the striatum at E14.5 while vessels were evenly dispersed without aggregates in both control and *Nrp1*$^{VEGF-}$ animals (Figure 4D-F). Finally, *Tie2-Cre;Nrp1*$^{fl/fl}$ animals had a significant decrease in vessel branching in the cortex at E14.5 while *Nrp1*$^{VEGF-}$ animals exhibited normal vessel branching (Figure 4G-I). Moreover, unlike the endothelial-specific NRP1 knock-out, the long term viability of the *Nrp1*$^{VEGF-}$ mutants allowed us to assess cortical vessel branching and coverage at P7 which was indistinguishable from control littermates (Figure 4G-I, Figure 4 – figure supplement 1).

NRP1 functions to modulate VEGFR2 levels independent of VEGF-NRP1 binding

The normal developmental angiogenesis observed in *Nrp1*$^{VEGF-}$ mutants clearly demonstrates that VEGF-NRP1 binding is not responsible for the vascular defects observed in *Nrp1*$^{-/-}$ or endothelial-specific NRP1 knockouts. In this regard, NRP1 must function through an alternative mechanism to regulate vascular development during embryogenesis. The intracellular domain of NRP1 does not have any obvious enzymatic activity and is not responsible for the signal transduction mediating angiogenesis (Fantin et al., 2011; Lanahan et al., 2013). Therefore, two apparent alternatives remain. One possibility is that a yet unidentified ligand outside the VEGF or SEMA3 family binds to NRP1 and instructs developmental angiogenesis. Alternatively, NRP1 may control vascular development by directly regulating its co-receptor, VEGFR2.

To directly test this second possibility, VEGFR2 expression was evaluated in *Tie2-Cre;Nrp1*$^{fl/-}$ mutants and control littermates via Western blot on E14.5 lung tissue. This biochemical assay revealed that total VEGFR2 protein levels were significantly reduced in *Tie2-Cre;Nrp1*$^{fl/-}$ mutants compared to their control littermates (Figure 5A-B). To determine the cell surface expression of VEGFR2 *in vivo*, we used fluorescence-activated cell sorting (FACS) to specifically quantify VEGFR2 expression at the cell surface of non-permeabilized endothelial cells derived from the acutely dissociated lungs of *Tie2-Cre;Nrp1*$^{fl/-}$ and control embryos. Remarkably, *Tie2-Cre;Nrp1*$^{fl/-}$ mutants displayed a significant decrease in the fluorescence intensity of VEGFR2 labeling as compared to control littermates (Figure 5E-F), suggesting that NRP1 functions to regulate VEGFR2 surface expression in endothelial cells. In contrast, both Western blot and FACS analysis determined that VEGFR2 protein levels were unperturbed in *Nrp1*$^{VEGF-}$ animals (Figure 5C-D,G-F). In addition, co-immunoprecipitation on P7 lung tissue revealed that NRP1 and VEGFR2 are physically associated in both control and *Nrp1*$^{VEGF-}$ animals (Figure 5 – figure supplement 1B), validating that NRP1-VEGFR2 receptor complex formation does not require VEGF-NRP1 binding *in vivo*. This result mimics our co-immunoprecipitation experiments on HEK293T cells transfected with either *WT Nrp1* or *Nrp1*^{D320K} constructs (Figure 5 – figure supplement 1A). Together, these findings indicate that NRP1 plays a role in regulating the cell surface expression of VEGFR2 in endothelial cells and that VEGF-NRP1 binding is not necessary for this function *in vivo* (Figure 5G).

To examine VEGF signaling in the *Tie2-Cre;Nrp1*$^{fl/-}$ and *Nrp1*$^{VEGF-}$ mutants, a VEGFR2 phosphorylation was performed on embryonic lung tissue isolated at E14.5 and quantified. Specifically, *Tie2-Cre;Nrp1*$^{fl/-}$ mutants had a severe reduction in VEGFR2 phosphorylation at the

tyrosine residue 1175 (Y1175) upon VEGF treatment (Figure 5 – figure supplement 2A,B). Interestingly, *Nrp1*$^{VEGF-}$ mutants also exhibited a mild reduction in VEGFR2 phosphorylation while total VEGFR2 protein levels were well maintained (Figure 5 – figure supplement 2C,D). Although the level of pVEGFR2 in the *Nrp1*$^{VEGF-}$ mutant was sufficiently high to support vascular development during embryogenesis, the modest reduction in pVEGFR2 may manifest in issues with angiogenesis, vascular maintenance and regeneration in the postnatal animal.

VEGF-NRP1 binding is required for postnatal angiogenesis

To directly test the role for VEGF-NRP1 binding in postnatal angiogenesis, wholemount immunostaining was performed with antibodies against isolectin and α-smooth muscle actin (α-SMA) to visualize the retinal blood vessels and arteries respectively. At P9, *Nrp1*$^{VEGF-}$ mutants exhibited a reduction in the vascular extension and artery number, but did not have any abnormalities in vessel coverage as compared with control littermates (Figure 6A). In the adult, the vascular extension and vessel coverage in the retina were indistinguishable from controls (Figure 6B) indicating that *Nrp1*$^{VEGF-}$ mutants experience a delay in the formation of the primary vascular plexus. However, the number of retinal arteries remained lower in *Nrp1*$^{VEGF-}$ adults. These results demonstrate that VEGF-NRP1 interactions are required to some degree for postnatal angiogenesis and artery differentiation in the retina.

In addition, *Nrp1*$^{VEGF-}$ animals were also assessed for injury-induced arteriogenesis following femoral artery ligation. In this assay, the femoral artery was surgically severed in both *Nrp1*$^{VEGF-}$ and controls and blood flow recovery was monitored via deep penetrating laser Doppler imaging. Femoral artery ligation produced a comparable level of hindlimb ischemia in *Nrp1*$^{VEGF-}$ mutants

and controls (Figure 6 – figure supplement 1). However, *Nrp1*$^{VEGF-}$ mutants exhibited a significant delay in hindlimb re-perfusion. Building upon these results, future work will utilize the *Nrp1*$^{VEGF-}$ knock-in line to determine if VEGF-NRP1 signaling functions in pathological or physiological angiogenesis in the adult.

Discussion

In this study, we identified a single amino acid within the extracellular b1 domain of NRP1 that is required for VEGF-NRP1 binding, but non-essential for SEMA3-NRP1 interactions. A point mutation in this D320 residue was incorporated into the endogenous *Nrp1* locus to generate the *Nrp1*$^{VEGF-}$ mutant, a novel mouse line that selectively abolishes VEGF-NRP1 binding *in vivo*. Recently a cDNA knock-in NRP1 mutant, *Nrp1*$^{Y297A/Y297A}$, was also developed to examine the role of VEGF-NRP1 binding (Fantin et al., 2014). However, mice generated with genetically modified cDNA notoriously lack the essential intronic regions that regulate the temporal and spatial expression of the gene. Consequently, the aberrant and severe down-regulation of NRP1 protein expression in the *Nrp1*$^{Y297A/Y297A}$ hypomorph prevents any definitive conclusions from being garnered about the biological cause of phenotypes present in this mouse. In this regard, abnormalities in the *Nrp1*$^{Y297A/Y297A}$ hypomorph could originate from two potential sources: the severe reduction in NRP1 levels or the abolishment of VEGF-NRP1 binding. Unlike the *Nrp1*$^{Y297A/Y297A}$ line, our *Nrp1*$^{VEGF-}$ mutant contains a two base pair replacement in the endogenous *Nrp1* locus and preserves the genetic structure of the *Nrp1* gene. Consequently, *Nrp1*$^{VEGF-}$ mice maintain appropriate levels of NRP1 protein expression and allow the first unobscured *in vivo* assessment of VEGF-NRP1 binding in developmental angiogenesis. In this

289 regard, our *Nrp1*$^{VEGF-}$ line provides a powerful new genetic tool for selectively interrogating the
290 function of VEGF-NRP1 binding in broad areas of basic research and translational study.
291
292 Remarkably, our *Nrp1*$^{VEGF-}$ mutant did not recapitulate the early embryonic lethality or
293 developmental angiogenesis phenotypes of the *Nrp1*$^{-/-}$ and endothelial-specific NRP1 knock-out
294 (Figure 4). Moreover, the *Nrp1*$^{VEGF-}$ mutant did not exhibit any of the cardiac failure, perinatal
295 lethality, or growth defects observed in the *Nrp1*$^{Y297A/Y297A}$ hypomorph indicating that these
296 phenotypes are attributed to the severe reduction in NRP1 protein in *Nrp1*$^{Y297A/Y297A}$ mutants
297 rather than the lack of VEGF-NRP1 binding. However, the *Nrp1*$^{VEGF-}$ mutant did exhibit a delay
298 in vascular extension and a reduction in the number of arteries in the postnatal retina. This retinal
299 phenotype is significantly less severe than those observed in the *Nrp1*$^{Y297A/Y297A}$ hypomorph
300 (Fantin et al., 2014) or in animals treated with antibodies inhibiting VEGF-NRP1 binding (Pan et
301 al., 2007). Together, these results reveal that the retina relies on both VEGF-NRP1 dependent
302 and independent mechanisms to establish the retinal vasculature.
303
304 Our surprising results challenge the well-accepted view that NRP1 depends on VEGF-NRP1
305 binding to facilitate angiogenesis and points to a provocative new hypothesis that NRP1
306 functions independently of VEGF-NRP1 binding perhaps via its interaction with an unidentified
307 ligand or in its capacity as a co-receptor for VEGFR2. Our study demonstrates the NRP1-
308 deficient endothelial cells have reduced VEGFR2 expression at the cell surface, a phenomenon
309 that was not observed in the *Nrp1*$^{VEGF-}$ mutants. This result provides the first *in vivo* evidence
310 that NRP1 controls VEGFR2 levels at the cell membrane and offers the first *in vivo* phenotypic
311 characterization linking NRP1 regulated VEGFR2 surface expression to vascular development.

Consistent with our *in vivo* observations, several lines of *in vitro* work using multiple cell culture systems demonstrate that NRP1 is essential for the proper presentation, recycling, and degradation of VEGFR2 (Shintani et al., 2006; Holmes et al., 2008; Ballmer-Hofer et al. 2011; Hamerlik et al., 2012) . Loss of function and gain of function studies in human umbilical vein endothelial cells (HUVECs) found that the VEGFR2 protein levels were decreased in the absence of NRP1 while *Vegfr2* mRNA levels were unaffected by Nrp1 siRNA (Shintani et al., 2006; Holmes et al., 2008). Similarly, Hamerlik et al. (2012) examined human glioblastoma multiforme cells and found that shRNA mediated knock-down of NRP1 resulted in dramatically decreased VEGFR2 protein levels accompanied by a lower surface presentation of VEGFR2 and a decrease in cell viability. Moreover, cell surface protein biotinylation and immunofluorescence staining with confocal microscopy confirmed the co-localization of VEGFR2-NRP1 with the early/recycling endosome. Finally, Ballmer-Hofer et al., 2011 used stably transfected porcine aortic endothelial cell (PAEC) lines in conjunction with immunostaining to visually follow VEGFR2 trafficking in the presence and absence of NRP1. Their experiments revealed that upon VEGF stimulation, VEGFR2 is internalized in Rab7 vesicles for degradation. However, in the presence of NRP1, VEGFR2 is stabilized in Rab11 vesicles and recycled back to the cell surface. In conjunction with our *in vivo* results, these data demonstrate that NRP1 guides vascular development through its capacity as a VEGFR2 co-receptor rather binding to VEGF. In this manner, NRP1 regulates angiogenesis by controlling the amount of VEGFR2 expression at the cell surface and consequently the level of VEGFR2-VEGF signaling.

The modulation of co-receptors may function as a general mechanism for regulating cell signaling and behavior. A prior *in vitro* study identified a similar relationship between the membrane protein, neural cell adhesion molecule (NCAM) and fibroblast growth factor receptor-1 (FGFR1) (Francavilla et al., 2009). This previous work discovered that NCAM induced sustained FGFR1 activation by controlling the intracellular trafficking of the FGFR1 receptor. Specifically, NCAM was capable of re-targeting internalized FGFR1 from the lysosomal degradation pathway to Rab11-postive recycling vesicles and increased FGFR1 expression at the cell surface. In this regard, the co-receptor interaction between NRP1 and VEGFR2 may be representative of a more universal phenomenon in which membrane proteins function to regulate the cell surface expression and subsequent downstream signaling of receptors.

Ultimately, our findings mark a pivotal step toward understanding the role of NRP1 in developmental angiogenesis and indicate that NRP1-VEGFR2 interactions rather than VEGF-NRP1 binding underlie NRP1's critical function in VEGF-mediated vascular development. Given the substantial resources invested in NRP1 targeted anti-angiogenesis therapies for vascular disease and cancer, the information gleaned from this study will be invaluable in identifying the cellular and molecular mechanisms underlying angiogenesis and ultimately using this information to instruct the development of new therapeutic approaches.

Materials and methods

Site-directed mutagenesis and targeting vector construction.

Rat Neuropilin1 cDNA was re-cloned from pMT21 into pCS2+ using the original EcoRI and XhoI sites present in both vectors. Mutations were made using PCR and the mutated fragment was subcloned back into pCS2-Nrp1 using endogenous restriction sites. The targeting vector

(TV) was constructed using a combination of traditional cloning and recombineering along with point mutagenesis. Genomic DNA was obtained from the 129S7-AB2.2 BAC library, clone #bMQ-373E22. The short (3') arm (1.3 kb) was cloned into the HpaI and EcoRI sites of 4600C-loxP. Two short homology arms (900 bp total) were created and cloned into the XhoI and NotI sites of 4600C-loxP, with the two arms joined by a SalI site. The homology arms were ligated in a triple ligation to 4600C-loxP as well as to each other. The vector was then linearized with SalI and electroporated into modified electrocompetent DH10B cells containing the previously mentioned BAC in order to facilitate homologous recombination to insert the remainder of the long arm. Recombineering was performed as described by the NCI-Frederick. After a full-length TV was made, the D320K mutation was introduced. The final TV was linerarized and electroporated into ES cells. All primer sequences used for the targeting vector construction are provided in Supplementary file 1.

Alkaline-phosphatase-tagged ligand production.

HEK293T cells were transfected with AP-SEMA3A, AP-VEGF A, AP-VEGF B, or AP-PlGF expression constructs using a calcium phosphate transfection method. Media was changed after 6 hours. Cells were cultured for an additional 48 hours in DMEM + 10% FBS. After 48 hours the media was collected, filtered to remove cell debris, and AP activity was measured. The ligands were frozen at -80°C until use.

Binding of AP-tagged protein to cells and unpermeabilized antibody staining.

COS-1 cells were grown in DMEM + 10% fetal bovine serum (FBS) + 1% Penicillin Streptomycin. Cells were transfected with the indicated expression vectors using Lipofectamine-

2000 (Invitrogen) in 6-well plates. 24 hours later, transfected cells were split into 24-well plates for parallel AP-binding and antibody staining. 24 hours after splitting, binding was performed using AP-tagged ligands (AP-VEGF A, AP-SEMA3A, AP-VEGF B, AP-PlGF). The binding protocol was as follows: cells were washed 1X with HBHA (1X HBSS, 0.5 mg/mL BSA, 0.5% sodium azide and 20 mM HEPES (pH 7)), then incubated for 75 minutes with 0.3 mL of 2 nM ligand. Cells were then washed 7X with HBHA on a rotating platform and 110 µl of cell lysis buffer (1% Triton X-100 and 10 mM Tris-HCl (pH 8)) was added to each well. Cells and buffer were scraped into Eppendorf tubes, then vortexed for 5 minutes to fully lyse them. The lysates were then spun down for 5 minutes, and the supernatant was heat inactivated at 65°C for 10 minutes to inactivate endogenous alkaline phosphatases. AP-activity was measured by adding 2X SEAP buffer (50mL 2M diethanolamine (pH 9.8), 50 µL 1M $MgCl_2$, 224 mg L-homoarginine, 50 mg BSA, 445 mg p-nitrophenylphosphate) and measuring optical absorbance at 405 nm every 15 seconds for one minute. Antibody staining of these cells was done as follows: non-specific binding was blocked with 5% Normal Goat Serum in DMEM for 30 minutes at 4°C. Cells were then incubated with primary antibody (Rabbit anti-Nrp1, gift of Dr. David Ginty) for 2 hours at 4°C. They were then washed 6X with cold HBHA, then incubated with a secondary antibody (AP-tagged anti-rabbit) for 1.5 hours at 4°C. Cells were then washed 3X in cold HBHA, then lysed as described above. AP-activity was measured from lysed extracts. Binding of AP-tagged ligands was normalized to protein content of each well and to antibody staining with an anti-NRP1 antibody. Each AP-binding assay was independently repeated at three times.

Animal care.

403 *Nrp1*$^{VEGF-}$, *Tie2*-Cre, *Nrp1*^{fl}, and *Nrp1*$^{-}$ (Gu et al., 2003) mice were maintained on a C57Bl/6
404 background. *Nrp1*$^{VEGF-}$ mice were genotyped with traditional PCR techniques. The expected WT
405 band is 305 bp, while the targeted allele is 350 bp due to the remaining presence of one FRT site.
406 To sequence the mutation site, PCR was performed to generate a fragment around the mutation
407 site. The primer sequences for genotyping and sequencing are included in Table 1. *Tie2-Cre*,
408 *Nrp1*^{fl} and *Nrp1*$^{-}$ genotyping was performed as previously published. All animals were treated
409 according to institutional and NIH guidelines approved by IACUC at Harvard Medical School.
410
411 *AP-ligand binding to tissue sections*.
412 Embryos were dissected and frozen immediately in liquid nitrogen, then stored at -80°C until
413 use. Sections were cut at 25 μm with a cryostat, then fixed for 8 minutes in ice-cold methanol.
414 Sections were then washed 3X in PBS + 4 mM $MgCl_2$. Non-specific binding was reduced by
415 blocking the sections with DMEM+ 10% FBS for 45 minutes. After fixation, sections were
416 incubated with 2 nM AP-tagged ligand diluted with PBS + 4 mM $MgCl_2$ and buffered with
417 HEPES, pH 7 for 1.5 hours at room temperature in a humidified chamber. The sections were
418 washed 5X in PBS + 4 mM $MgCl_2$, then fixed with a fixative solution (60% acetone, 1%
419 formaldehyde, 20 mM HEPES, pH 7). Sections were washed 3X in PBS and incubated in PBS at
420 65°C for 2 hours to heat inactive endogenous alkaline phosphatases and then incubated overnight
421 in developing solution (100 mM Tris-HCl pH 9.5, 100 mM NaCl, 5 mM $MgCl_2$) with NBT
422 (nitro-blue tetrazolium chloride) and BCIP (5-bromo-4-chloro-3'-indolyphosphate p-toluidine).
423 AP-ligand binding was analyzed in sections from at least three animals across two different
424 litters per genotype.
425

Western blotting.

For immunoblotting, E14.5 lung samples were loaded on 8% polyacrylamide gels and run until the appropriate protein separation was achieved. Samples were electrophoretically transferred onto PVDF membrane. Non-specific binding was blocked by a one hour incubation in 5% non-fat milk in TBST (Tris-buffered saline + 0.1% Tween-20). The membranes were then incubated overnight with the following primary antibodies, as indicated below, at 4°C: anti-NRP1 (Abcam #ab81321 or gift of Dr. David Ginty, see (Ginty et al., 1993) for details), anti-VEGFR2 (gift of Procter and Gamble, see (Gu et al., 2003) for details), anti-VE-cadherin (Abcam #ab33168), anti-p-VEGFR2 (p1175) (Cell Signaling Tech. #2478), and anti-α-Tubulin (Sigma #T5168). After incubation with primary antibodies, the membranes were washed 3X in TBST then incubated with the appropriate HRP-labeled secondary antibody in TBST or 5% milk in TBST for one hour at room temperature. Membranes were then washed 3X with TBST then developed with regular or super ECL (GE Amersham or Thermo Scientific). The intensity of individual bands was quantified using ImageJ.

Phenotypic analysis of the $Nrp1^{VEGF-}$ mutant

At the indicated stages, embryos were dissected, fixed with 4% paraformaldehyde, equilibrated in a sucrose gradient, embedded in OCT, and sectioned in the coronal plan at 12 µm with a Leica CM3050S cryostat. Likewise, the brains of postnatal pups (P7) were dissected, fixed, cryo-protected, and sectioned at 20 µm. Tissue sections were washed 3X 5 minutes in 0.2% PBT (0.2% Triton X-100 in PBS), incubated with Isolectin GS-IB4 (Life Technologies #I21411) overnight at 4°C, washed 3X 5 minutes in PBS, and coverslipped with using ProLong Gold/DAPI antifade reagent (Molecular Probes #P36935). Sections were imaged by fluorescence

449 microscopy using a Nikon Eclipe 80i microscope equipped with a Nikon DS-2 digital camera.
450 Quantification was performed using ImageJ. Vessel coverage delineates the percent of cortical
451 pixel area covered by isolectin-positive pixels while vessel size quantifies the pixel area of each
452 discrete vascular aggregate identified by isolectin staining.
453
454 *VEGF lung treatment*.
455 E14.5 mouse lungs were dissected in cold PBS, and minced finely using a razor blade. The tissue
456 was then incubated with plain EBM (Lonza) or EBM containing 50 ng/ml VEGF for 15 minutes
457 at 37°C. Lysis buffer (50 mM Tris/HCl (pH 7.5), 150 mM NaCl, 1% Triton X-100, 2mM EDTA
458 and 2mM DTT) containing complete proteinase inhibitors (Roche), PhosSTOP (Roche) and
459 sodium orthovanadate was added to the tissue, which was then pulverized with a pestle and
460 incubated for 30 minutes while rotating at 4°C. Tissue was spun down and protein quantification
461 was performed. The tissue was treated as described in the western blotting section.
462
463 *Co-immunoprecipitation*.
464 HEK293T cells were transfected with the indicated constructs using Lipofectamine-2000
465 (Invitrogen). They were then grown in DMEM + 10% fetal bovine serum + 1% Penicillin
466 Streptomycin, and 48 hours after transfection, cells were washed and harvested in ice-cold PBS.
467 Cells were lysed using lysis buffer (50 mM Tris/HCl (pH 7.5), 150 mM NaCl, 1% Triton X-100,
468 2mM EDTA and 2mM DTT) containing complete proteinase inhibitors (Roche). After 30
469 minutes of rotation in the cold room and subsequent centrifugation, protein was quantified and
470 20 μg of protein was frozen down as input controls. 0.5 μg of anti-VEGFR2 antibody (gift of
471 Procter and Gamble, see (Gu et al., 2003) for details) was added to 500 μg of protein and rotated

in the cold room for one hour. Then, 20 µL of Protein A/G beads (Thermo Scientific) were added to the protein and rotated overnight in the cold room. Beads were washed 3X with lysis buffer and two times with wash buffer (lysis buffer with 300 mM NaCl). Protein was eluted by the addition of 2X SDS-PAGE sample buffer and boiling for 10 minutes. Co-immunoprecipitation was also performed on P7 lung lysates isolated from control and $Nrp1^{VEGF-}$ animals treated with VEGF as described above.

FACS.

Analysis of E14.5 mouse embryos were performed on single cells from dissociated lungs. In brief, microdissection techniques were used to isolate the lung. Lungs were then rinsed in PBS, and incubated in 2mg/ml collagenase and 20 µg/ml DNase I 3X for 15 minutes at 37°C and gently pipetted. The collagenase was inactivated using 5 ml of ice-cold 10% FBS/PBS, centrifuged at 1,000g for 5 minutes, and suspended in 400µl of red blood cell (RBC) lysis buffer (Sigma). Following a 5 minutes incubation at RT, 2 ml of ice-cold 5% FBS/PBS was added and cells were centrifuged at 1,000g for 5 minutes at 4°C. Cells were then blocked in Fc-blocking solution (BD #553142) for 20 minutes on ice, centrifuged, incubated with the labeled conjugated primary antibodies- PE-anti-CD31 (PECAM) (BD #553373) and APC-anti-Flk1-1 (VEGFR2) (BD #560070), for 30 minutes on ice with agitation every 10 minutes. After incubation the cells were spun down, the supernatant was removed and the cell pellet was resuspend in 1:10K Sytox in PBS/5%FBS. Cells were analyzed on LSR II Flow Cytometer. Cells incubated with no antibody, APC-anti-Flk1, or PE-anti-CD31 only served as the control population.

Phenotypic analysis of the developing retina

Whole mount retina immunohistochemistry was performed as previously described in Kim et al., 2011. Briefly, eyes were extracted and fixed in 4% paraformaldehyde for 10 minutes at room temperature. Retinas were dissected in PBS, post-fixed in 4% paraformaldehyde overnight at 4°C. Retinas were then permeabilized in PBS, 1% BSA, and 0.5% Triton X-100 at 4°C overnight, washed 2X 5 minutes in 1% PBT (1% Triton X-100 in PBS), and incubated in Isolectin GS-IB4 (1:200, Life Technologies #I21411) and anti- αSMA Cy3 (1:100, Sigma #C6198) in 1% PBT overnight at 4°C. Retinas were washed 3X 5 minutes and flat mounted using ProLong Gold antifade reagent (Molecular Probes #P36934). Flat mounted retinas were analyzed by fluorescence microscopy using a Nikon Eclipe 80i microscope equipped with a Nikon DS-2 digital camera and by confocal laser scanning microscopy using an Olympus FV1000 confocal microscope. Quantification was performed using MetaMorph Image Analysis Software and ImageJ. At least four retinal leafs were quantified per animal to determine the vascular extension ratio, both eyes were examined in each animal for artery number, and three representative images were quantified from each animal for vascular coverage (representing the total isolectin-positive pixel area per image).

Femoral Artery Ligation

Ketamine (80-100mg/kg) and xylazine (5-10 mg/kg) delivered by IP injection were used to anesthetize 12 week old male $Nrp1^{VEGF-}$ and control littermates. After anesthesia was achieved, the bilateral hind limbs and lower abdomen were cleared of hair and cleaned with 10% betadine and 70% alcohol. An incision of 3-4 mm was made in the right inguinal area to visualize the femoral artery. Two 6-0 silk sutures were tied in the proximal femoral artery and the deep femoral and epigastric artery branches were cauterized. The femoral artery was then ligated

between the two sutures. The skin was sutured with one 4-0 prolene sutures. Immediately before and after surgery, each animal was scanned with a non-invasive laser doppler imaging system (Moor Instruments; moorLD12-HR) under 1-3% isofluorane anesthesia. Blood flow recovery in the hind limbs was further assessed on 3, 5, and 7 days postsurgery and quantified via Moor LDI Software.

Statistical analysis.

The standard error of the mean was calculated for each experiment and error bars in the graphs represent the standard error. A paired Student's *t* test was used to determine the statistical significance of differences between samples and the genotype distribution was analyzed using a Chi-square test. Statistical analyses were performed with Prism 4 (GraphPad Software) and p values are indicated by * ≤ 0.05, ** ≤ 0.01, and *** ≤ 0.001.

Acknowledgements

We thank members of the Gu laboratory for helpful comments on the manuscript, Lauren Byrnes for technical support, and both the Flow Cytometry Facility in the Systems Biology Department and the Neurobiology Imaging Facility in the Neurobiology Department of Harvard Medical School for consultation and instrument availability that facilitated this work. The Neurobiology Imaging Facility is supported in part by the Neural Imaging Center as part of an NINDS P30 Core Center grant #NS072030. This study was supported by the National Institutes of Health Fundamental Neurobiology Training grant T32 NS007484-12 (N. Hagan), the Alice and Joseph Brooks Fund Postdoctoral Fellowship (A. Tata), Harvard Mahoney Neuroscience Institute Fund Postdoctoral Fellowship (B. Lacoste), National Institutes of Health grant R01 HL096384 (K.

Kang and J. Bischoff), and the following grants to C. Gu: Sloan research fellowship, Armenise junior faculty award, the Genise Goldenson fund, and National Institutes of Health grant R01 NS064583.

References

Ballmer-Hofer, K., Andersson, A.E., Ratcliffe, L.E., and Berger, P. (2011). Neuropilin-1 promotes VEGFR-2 trafficking through Rab11 vesicles thereby specifying signal output. Blood *118*, 816–826.

Carmeliet, P., Ferreira, V., Breier, G., Pollefeyt, S., Kieckens, L., Gertsenstein, M., Fahrig, M., Vandenhoeck, A., Harpal, K., Eberhardt, C., et al. (1996). Abnormal blood vessel development and lethality in embryos lacking a single VEGF allele. Nature *380*, 435–439.

Carmeliet, P., Ng, Y.S., Nuyens, D., Theilmeier, G., Brusselmans, K., Cornelissen, I., Ehler, E., Kakkar, V.V., Stalmans, I., Mattot, V., et al. (1999). Impaired myocardial angiogenesis and ischemic cardiomyopathy in mice lacking the vascular endothelial growth factor isoforms VEGF164 and VEGF188. Nat. Med. *5*, 495–502.

Chung, A.S., and Ferrara, N. (2011). Developmental and pathological angiogenesis. Annu. Rev. Cell Dev. Biol. *27*, 563–584.

Coultas, L., Chawengsaksophak, K., and Rossant, J. (2005). Endothelial cells and VEGF in vascular development. Nature *438*, 937–945.

Fantin, A., Schwarz, Q., Davidson, K., Normando, E.M., Denti, L., and Ruhrberg, C. (2011). The cytoplasmic domain of neuropilin 1 is dispensable for angiogenesis, but promotes the spatial separation of retinal arteries and veins. Dev. Camb. Engl. *138*, 4185–4191.

Fantin, A., Herzog, B., Mahmoud, M., Yamaji, M., Plein, A., Denti, L., Ruhrberg, C., and Zachary, I. (2014). Neuropilin 1 (NRP1) hypomorphism combined with defective VEGF-A binding reveals novel roles for NRP1 in developmental and pathological angiogenesis. Dev. Camb. Engl. *141*, 556–562.

Ferrara, N., Carver-Moore, K., Chen, H., Dowd, M., Lu, L., O'Shea, K.S., Powell-Braxton, L., Hillan, K.J., and Moore, M.W. (1996). Heterozygous embryonic lethality induced by targeted inactivation of the VEGF gene. Nature *380*, 439–442.

Ferrara, N., Gerber, H.-P., and LeCouter, J. (2003). The biology of VEGF and its receptors. Nat. Med. *9*, 669–676.

Francavilla, C., Cattaneo, P., Berezin, V., Bock, E., Ami, D., de Marco, A., Christofori, G., and Cavallaro, U. (2009). The binding of NCAM to FGFR1 induces a specific cellular response mediated by receptor trafficking. J. Cell Biol. *187*, 1101–1116.

Ginty, D.D., Kornhauser, J.M., Thompson, M.A., Bading, H., Mayo, K.E., Takahashi, J.S., and Greenberg, M.E. (1993). Regulation of CREB phosphorylation in the suprachiasmatic nucleus by light and a circadian clock. Science *260*, 238–241.

Gu, C., Limberg, B.J., Whitaker, G.B., Perman, B., Leahy, D.J., Rosenbaum, J.S., Ginty, D.D., and Kolodkin, A.L. (2002). Characterization of neuropilin-1 structural features that confer

binding to semaphorin 3A and vascular endothelial growth factor 165. J. Biol. Chem. *277*, 18069–18076.

Gu, C., Rodriguez, E.R., Reimert, D.V., Shu, T., Fritzsch, B., Richards, L.J., Kolodkin, A.L., and Ginty, D.D. (2003). Neuropilin-1 conveys semaphorin and VEGF signaling during neural and cardiovascular development. Dev. Cell *5*, 45–57.

Hamerlik, P., Lathia, J.D., Rasmussen, R., Wu, Q., Bartkova, J., Lee, M.H., Moudry, P., Kartek Jr., J., Fischer, W., Lukas, J., Rich, J.N., and Bartek, J. (2012). Autocrine VEGF-VEGFR2-Neuropilin-1 signaling promotes glioma stem-like cell viability and tumor growth. J. Exp. Med. *209*, 507-520.

He, Z., and Tessier-Lavigne, M. (1997). Neuropilin is a receptor for the axonal chemorepellent Semaphorin III. Cell *90*, 739–751.

Herzog, B., Pellet-Many, C., Britton, G., Hartzoulakis, B., and Zachary, I.C. (2011). VEGF binding to NRP1 is essential for VEGF stimulation of endothelial cell migration, complex formation between NRP1 and VEGFR2, and signaling via FAK Tyr407 phosphorylation. Mol. Biol. Cell *22*, 2766–2776.

Holmes, D.I.R., and Zachary, I.C. (2008). Vascular endothelial growth factor regulates stanniocalcin-1 expression via neuropilin-1-dependent regulation of KDR and synergism with fibroblast growth factor-2. Cell. Signal. *20*, 569–579.

Iruela-Arispe, M.L., and Dvorak, H.F. (1997). Angiogenesis: a dynamic balance of stimulators and inhibitors. Thromb. Haemost. *78*, 672–677.

Jaalouk, D.E., Ozawa, M.G., Sun, J., Lahdenranta, J., Schlingemann, R.O., Pasqualini, R., and Arap, W. (2007). The original Pathologische Anatomie Leiden-Endothelium monoclonal antibody recognizes a vascular endothelial growth factor binding site within neuropilin-1. Cancer Res. *67*, 9623–9629.

Kawasaki, T., Kitsukawa, T., Bekku, Y., Matsuda, Y., Sanbo, M., Yagi, T., and Fujisawa, H. (1999). A requirement for neuropilin-1 in embryonic vessel formation. Dev. Camb. Engl. *126*, 4895–4902.

Kim, J., Oh, W., Gaiano, N., Yoshida, Y., Gu, C., (2011). Semaphorin 3E-Plexin-D1 signaling regulates VEGF function in developmental angiogenesis via a feedback mechanism. Genes Dev. *25(13)* 1399-1411.

Kitsukawa, T., Shimizu, M., Sanbo, M., Hirata, T., Taniguchi, M., Bekku, Y., Yagi, T., and Fujisawa, H. (1997). Neuropilin-semaphorin III/D-mediated chemorepulsive signals play a crucial role in peripheral nerve projection in mice. Neuron *19*, 995–1005.

Kolodkin, A.L., Levengood, D.V., Rowe, E.G., Tai, Y.T., Giger, R.J., and Ginty, D.D. (1997). Neuropilin is a semaphorin III receptor. Cell *90*, 753–762.

Lanahan, A., Zhang, X., Fantin, A., Zhuang, Z., Rivera-Molina, F., Speichinger, K., Prahst, C., Zhang, J., Wang, Y., Davis, G., et al. (2013). The neuropilin 1 cytoplasmic domain is required for VEGF-A-dependent arteriogenesis. Dev. Cell *25*, 156–168.

Maes, C., Stockmans, I., Moermans, K., Van Looveren, R., Smets, N., Carmeliet, P., Bouillon, R., and Carmeliet, G. (2004). Soluble VEGF isoforms are essential for establishing epiphyseal vascularization and regulating chondrocyte development and survival. J. Clin. Invest. *113*, 188–199.

Miquerol, L., Gertsenstein, M., Harpal, K., Rossant, J., and Nagy, A. (1999). Multiple developmental roles of VEGF suggested by a LacZ-tagged allele. Dev. Biol. *212*, 307–322.

Olsson, A.-K., Dimberg, A., Kreuger, J., and Claesson-Welsh, L. (2006). VEGF receptor signalling - in control of vascular function. Nat. Rev. Mol. Cell Biol. *7*, 359–371.

Pan, Q., Chanthery, Y., Liang, W.-C., Stawicki, S., Mak, J., Rathore, N., Tong, R.K., Kowalski, J., Yee, S.F., Pacheco, G., et al. (2007). Blocking neuropilin-1 function has an additive effect with anti-VEGF to inhibit tumor growth. Cancer Cell *11*, 53–67.

Rossant, J., and Hirashima, M. (2003). Vascular development and patterning: making the right choices. Curr. Opin. Genet. Dev. *13*, 408–412.

Ruhrberg, C., Gerhardt, H., Golding, M., Watson, R., Ioannidou, S., Fujisawa, H., Betsholtz, C., and Shima, D.T. (2002). Spatially restricted patterning cues provided by heparin-binding VEGF-A control blood vessel branching morphogenesis. Genes Dev. *16*, 2684–2698.

Shintani, Y., Takashima, S., Asano, Y., Kato, H., Liao, Y., Yamazaki, S., Tsukamoto, O., Seguchi, O., Yamamoto, H., Fukushima, T., et al. (2006). Glycosaminoglycan modification of neuropilin-1 modulates VEGFR2 signaling. EMBO J. *25*, 3045–3055.

Soker, S., Takashima, S., Miao, H.Q., Neufeld, G., and Klagsbrun, M. (1998). Neuropilin-1 is expressed by endothelial and tumor cells as an isoform-specific receptor for vascular endothelial growth factor. Cell *92*, 735–745.

Stalmans, I., Ng, Y.-S., Rohan, R., Fruttiger, M., Bouché, A., Yuce, A., Fujisawa, H., Hermans, B., Shani, M., Jansen, S., et al. (2002). Arteriolar and venular patterning in retinas of mice selectively expressing VEGF isoforms. J. Clin. Invest. *109*, 327–336.

Vander Kooi, C.W., Jusino, M.A., Perman, B., Neau, D.B., Bellamy, H.D., and Leahy, D.J. (2007). Structural basis for ligand and heparin binding to neuropilin B domains. Proc. Natl. Acad. Sci. U. S. A. *104*, 6152–6157.

Figure Legends

Figure 1. Design and assessment of *Nrp1* variants harboring mutations in the VEGF-binding site (A) Schematic representation of the NRP1 b1 extracellular domain and crystal structure highlighting three potential mutagenesis sites: the PAL-E binding site (orange circle), tuftsin binding site (blue circle), and electronegative surface (red circle). **(B)** Sequence of the *Nrp1* b1 domain indicating the deletion or mutation sites for the candidate constructs. **(C)** AP-SEMA3A (top row) or AP-VEGF (middle row) binding to COS-1 cells overexpressing the indicated constructs. Deletion of the entire PAL-E binding site ($Nrp1^{PAL\text{-}E\Delta 7}$) or partial deletion of the PAL-E binding site ($Nrp1^{PAL\text{-}E\Delta 6}$ and $Nrp1^{PAL\text{-}E\ \Delta 5}$) eliminated both AP-SEMA3A and AP-VEGF binding. Likewise, mutations in the tuftsin binding site (S346A, E348A, T349A or S346A, E348A) abolished AP-SEMA3A binding and reduced AP-VEGF binding. Although mutations in the NRP1 electronegative surface (E319K, D320K) eliminated AP-VEGF binding and reduced AP-SEMA3A binding, the E319K mutation only slightly reduced AP-SEMA3A binding and maintained AP-VEGF binding. Antibody staining of unpermeabilized cells (lower row) demonstrated normal NRP1 surface expression. Scale bar: 50μm

Figure 1 – figure supplement 1: Assessment of additional *Nrp1* variants containing mutations in the VEGF-binding site. AP-SEMA3A or AP-VEGF was applied to COS-1 cells overexpressing the indicated construct (top and middle row). Non-permeabilized antibody staining was performed with a polyclonal anti-NRP1 antibody to detect surface expression of NRP1 (bottom row). Scale bar: 50μm

Figure 2. The $Nrp1^{D320K}$ mutant selectively eliminates VEGF-NRP1 binding *in vitro*. (A) AP-VEGF binding in COS-1 cells overexpressing the indicated *Nrp1* construct. WT NRP1

673 bound AP-VEGF strongly, while AP-VEGF binding to NRP1^{D320K} was abolished. Scale bar:
674 100μm **(B)** Western blot shows that equivalent levels of NRP1 protein in COS-1 cells transfected
675 with the *WT Nrp1* and *Nrp1^{D320K}*. **(C)** Quantification of the binding assay shows that AP-VEGF-
676 NRP1^{D320K} binding was abolished even after normalization for protein content and NRP1
677 expression. **(D)** Quantification of AP-SEMA3A binding comparable AP-SEMA3A binding in
678 WT NRP1 and NRP1^{D320K}. **(E)** Measurement of the dissociation constant (K_D) of AP-SEMA3A
679 demonstrates that AP-SEMA3A bound to the NRP1^{D320K}/PlexA4 complex with the same affinity
680 as the NRP1/PlexA4 complex.
681
682 **Figure 2 – figure supplement 1: VEGFA, VEGFB, and PLFG binding to NRP1 was**
683 **abolished in the *Nrp1^{D320K}* mutant.** *Nrp1* constructs were overexpressed in COS-1 cells and
684 AP-VEGFB or AP-PlGF was applied to cells to observe ligand binding. WT NRP1 bound AP-
685 VEGFB, and AP-PlGF strongly, while these ligands did not bind to NRP1^{D320K}. Scale bar:
686 100μm
687
688 **Figure 3: *Nrp1^{VEGF-}* mice selectively abolish VEGF-NRP1 binding *in vivo*. (A)** Targeting
689 vector design for the generation of *Nrp1^{VEGF-}* mice. The WT genomic region contained residue
690 D320 in exon 6 of *Nrp1*. The targeting vector (TV) introduced the D320K mutation along with
691 an Frt-flanked NeoR cassette to form the targeted allele (TA). After FlpE-mediated excision of
692 the NeoR cassette, the final targeted allele (FTA) had the D320K mutation as well as one
693 remaining Frt site. **(B)** Section binding assays demonstrated that AP-VEGF binding to the dorsal
694 root entry zone (DREZ) was abolished in *Nrp1^{VEGF-}* mutants (arrows, left panels) while AP-
695 SEMA3A binding to the DREZ appeared similar between *Nrp1^{VEGF-}* and control animals

(arrows, middle panels). Scale bar: 100μm **(C)** Western blot from E14.5 lung tissue shows that NRP1 protein level was not affected in *Nrp1*$^{VEGF-}$ animals. **(D-E)** *Nrp1*$^{VEGF-}$ mutants appear indistinguishable from controls littermates at embryonic (E14.5) and adult stages **(F)** *Nrp1*$^{VEGF-}$ mutants exhibit normal body weight in adulthood (n=7, males).

Figure 3 – figure supplement 1: Screening and verification of ES cells for the generation of the *Nrp1*$^{VEGF-}$ mutant.

(A) Diagram of the *Nrp1* genomic region following successful homologous recombination to insert the targeting vector. The green arrows indicate the primers used in B, while the blue arrows represent the primers used in C. **(B)** PCR screening for the proper insertion of the 3' homology arm. The 5' primer was located in the NeoR sequence while the 3' primer bound to an area outside of the targeting vector. Therefore, WT colonies did not produce a band, while correctly targeted clones produced a band of 1.7 kb. **(C)** PCR screening for the proper insertion of the 5' homology arm. The 5' primer was located outside of the targeting vector area and the 3' primer was located within the genomic sequence present in the 3' homology arm. Thus, PCR from a properly targeted clone produced a fragment that was 1.5 kb larger than a negative colony. **(D)** Sequencing of the D320K region in WT and *Nrp1*$^{VEGF-}$ homozygous mutants. The boxed region indicates the altered codon.

Figure 3 – figure supplement 2: *Nrp1*$^{VEGF-}$ mutant mice exhibit normal gross morphology.

(A) Whole mount images of the heart at P9 show the normal cardiac morphology of *Nrp1*$^{VEGF-}$ mutants. **(B-C)** Organ weights measured at P9 (B) and adulthood (C) demonstrate the heart, brain, lung, and kidney undergo appropriate growth in *Nrp1*$^{VEGF-}$ animals, n≥5 **(D)** Western blots

from adult heart, brain, lung, and kidney tissue demonstrate that NRP1 protein level was not affected in *Nrp1*$^{VEGF-}$ animals. **(E)** Viability table depicts the predicted and observed frequencies for each genotype at the indicated developmental stages. The table values represent the percentage of the total number of animals genotyped per age while the total number of animals is shown in parentheses.

Figure 4: VEGF-NRP1 binding is not required for developmental angiogenesis (A) Vessel immunostaining with isolectin (green) revealed that *Tie2-Cre;Nrp1*$^{fl/fl}$ mutants had delayed vessel ingression into the cerebral cortex at E11.5 while *Nrp1*$^{VEGF-}$ mutants exhibited normal ingression. DAPI was used to stain the nuclei (blue). **(B-C)** Quantification of cortical vessel ingression shown in A, n=3. **(D)** *Tie2-Cre;Nrp1*$^{fl/fl}$ mutants exhibited large vessel clumps in the brain (particularly in the striatum) at E14.5, a phenotype not observed in *Nrp1*$^{VEGF-}$ mutants. **(E-F)** Quantification of vessel size in E14.5 striatum shown in D, n=3. **(G)** *Tie2-Cre;Nrp1*$^{fl/fl}$ mutants have reduced vessel branching in the cerebral cortex while *Nrp1*$^{VEGF-}$ mutants displayed normal vessel branching at E14.5. **(H-I)** Quantification of vessel branching in E14.5 cortex shown in G, n=4. Scale bar: 200μm

Figure 4 – figure supplement 1: *Nrp1*$^{VEGF-}$ mutant mice display normal vessel branching and coverage at postnatal stages (A) Vessel immunostaining with isolectin (green) demonstrates that *Nrp1*$^{VEGF-}$ mutants have normal vessel coverage and branching in the cerebral cortex at P7. **(B-C)** Quantification of vessel coverage and branching in P7 cortex shown in A, n=3. Scale bar: 200μm

Figure 5: NRP1 regulates VEGFR2 expression at the cell surface independent of VEGF-NRP1 binding. **(A)** Western blot from E14.5 lung tissue treated with 50 ng/ml VEGF for 15 minutes revealed that VEGFR2 was reduced in *Tie2-CreNrp1*$^{fl/-}$ mutants while VE-cadherin expression remained at controls levels. Western blot for NRP1 demonstrates that the *Tie2-Cre* allele successfully knocked down NRP1 expression. **(B)** Quantification of VEGFR2 expression shown in A, n=4 **(C)** Western blot from E14.5 lung tissue treated with 50 ng/ml VEGF for 15 minutes demonstrates that VEGFR2, NRP1, and VE-cadherin expression were unperturbed in *Nrp1*$^{VEGF-}$ mutants. **(D)** Quantification of VEGFR2 expression shown in C, n=5 **(E)** FACS analysis plots illustrate a reduction in VEGFR2 surface expression in endothelial cells isolated from *Tie2-Cre;Nrp1*$^{fl/-}$ mice. **(F)** Quantification of the VEGFR2 fluorescence intensity from the FACS analysis shown in E, n=5. **(G)** FACS analysis plots demonstrate that VEGFR2 surface expression in in endothelial cells isolated from *Nrp1*$^{VEGF-}$ mice remained at control levels. **(H)** Quantification of the VEGFR2 fluorescence intensity from the FACS analysis shown in G, n≥7. **(I)** Schematic of VEGFR2 and NRP1 at the cell surface illustrates VEGF ligand binding to both VEGFR2 and Nrp1. In *Nrp1*$^{VEGF-}$ mutants, VEGF-NRP1 binding is abolished, VEGFR2 has normal cell surface localization, and vascular development proceeds appropriately. However, in *Nrp1*$^{-/-}$ mutants, VEGFR2 cell surface localization is reduced and vascular development is impaired.

Figure 5 – figure supplement 1: VEGF-Nrp1 binding is not required for Nrp1-VEGFR2 complex formation *in vitro* and *in vivo*. **(A)** HEK293T cells transfected with *Vegfr2* and either *WT Nrp1* or *Nrp1*^{D230K} exhibited normal NRP1-VEGFR2 complex formation. **(B)** Lung lysates

764 generated from *Nrp1*$^{VEGF-}$ mutants also displayed normal NRP1-VEGFR2 complex formation
765 comparable to littermate controls.
766
767 **Figure 5 – figure supplement 2: VEGF-induced VEGFR2 phosphorylation is reduced in**
768 **both *Nrp1*$^{VEGF-}$ and *Tie2-Cre;Nrp1*$^{fl/-}$ mutants.**
769 **(A)** Western blot from E14.5 lung tissue shows that VEGFR2 phosphorylation upon VEGF
770 treatment was diminished in the *Nrp1*$^{VEGF-}$ mutant. **(B)** Quantification of VEGFR2
771 phosphorylation shown in A, n=7. **(C)** Western blot from E14.5 lung tissue demonstrates that
772 VEGFR2 phosphorylation is significantly reduced in *Tie2-Cre;Nrp1*$^{fl/-}$ mutants. **(D)**
773 Quantification of VEGFR2 phosphorylation shown in B, n=5.
774
775 **Figure 6: Retinal angiogenesis is perturbed in the *Nrp1*$^{VEGF-}$ mutant**
776 **(A)** Isolectin and α-SMA immunostaining on P9 retinal flatmounts revealed a significant
777 reduction in vascular extension and artery number in *Nrp1*$^{VEGF-}$ mutants. However, vessel
778 coverage in the retina was unperturbed in the *Nrp1*$^{VEGF-}$ mutants, n=6. **(B)** In the adult, isolectin
779 and α-SMA immunostaining showed that the number of retinal arteries remained lower in
780 *Nrp1*$^{VEGF-}$ mutants than littermate controls while vascular extension and vessel coverage in the
781 retina were normal, n=4. Scale bar: 200μm
782
783 **Figure 6 – figure supplement 1: *Nrp1*$^{VEGF-}$ mutants have delayed blood flow recovery**
784 **following femoral artery ligation.**
785 **(A)** Laser doppler imaging demonstrates severe hind-limb ischemia directly after femoral artery
786 ligation in both control and *Nrp1*$^{VEGF-}$ animals (arrows). Five days after surgery, blood flow

787 recovery in the injured hind-limb was significantly greater in control versus *Nrp1*$^{VEGF-}$ animals

788 (arrowheads). **(B)** Quantification of blood flow recovery following femoral artery ligation, n=7.

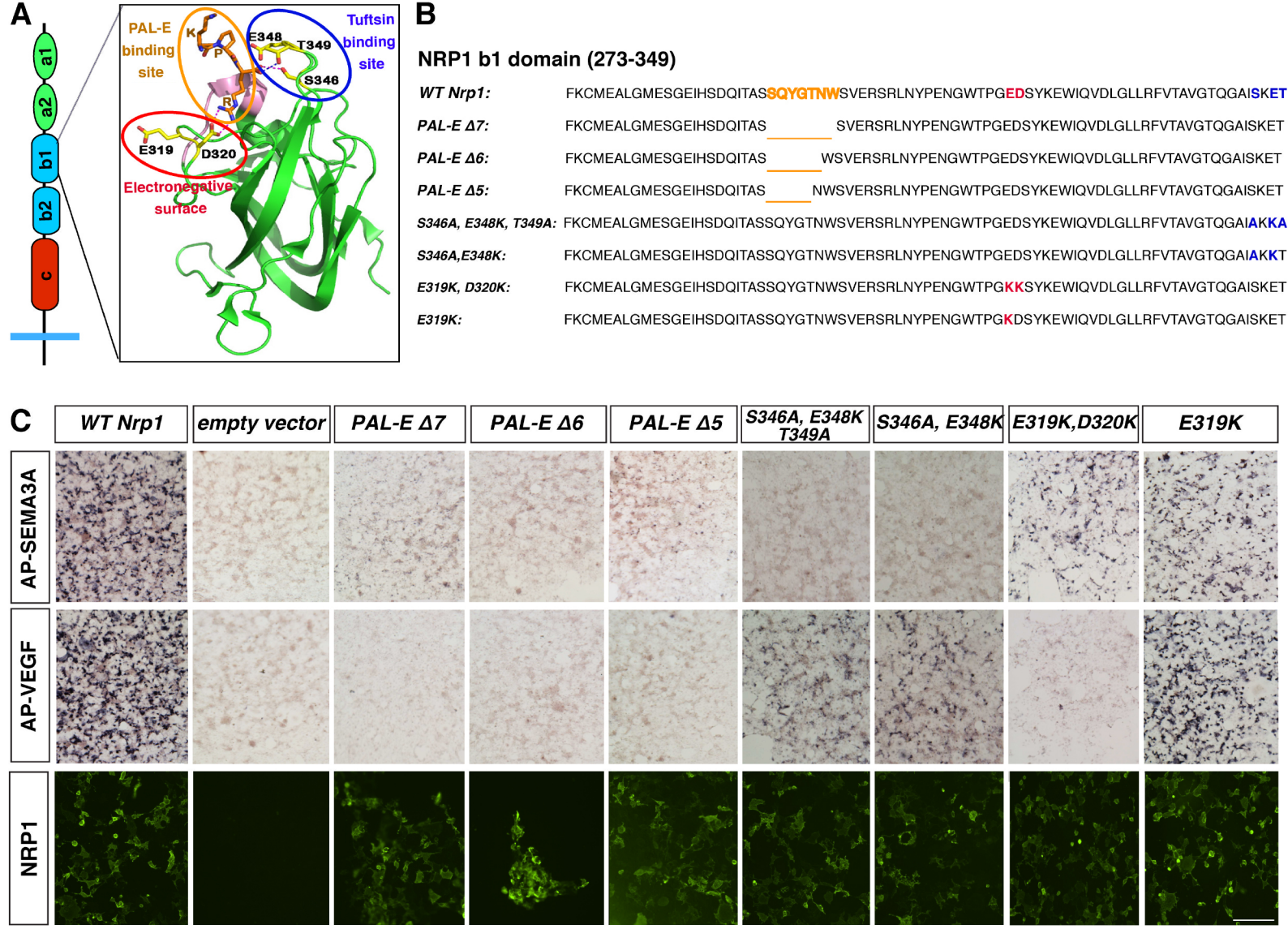
A
a1
a2
b1
b2
c
PAL-E binding site
Tuftsin binding site
K
P
R
E348
T349
S346
E319
D320
Electronegative surface
B
NRP1 b1 domain (273-349)
WT Nrp1: FKCMEALGMESGEIHSDQITASSQYGTNWSVERSRLNYPENGWTPGEDSYKEWIQVDLGLLRFVTAVGTQGAISKET
PAL-E Δ7: FKCMEALGMESGEIHSDQITAS SVERSRLNYPENGWTPGEDSYKEWIQVDLGLLRFVTAVGTQGAISKET
PAL-E Δ6: FKCMEALGMESGEIHSDQITAS WSVERSRLNYPENGWTPGEDSYKEWIQVDLGLLRFVTAVGTQGAISKET
PAL-E Δ5: FKCMEALGMESGEIHSDQITAS NWSVERSRLNYPENGWTPGEDSYKEWIQVDLGLLRFVTAVGTQGAISKET
S346A, E348K, T349A: FKCMEALGMESGEIHSDQITASSQYGTNWSVERSRLNYPENGWTPGEDSYKEWIQVDLGLLRFVTAVGTQGAIAKKA
S346A,E348K: FKCMEALGMESGEIHSDQITASSQYGTNWSVERSRLNYPENGWTPGEDSYKEWIQVDLGLLRFVTAVGTQGAIAKKT
E319K, D320K: FKCMEALGMESGEIHSDQITASSQYGTNWSVERSRLNYPENGWTPGKKSYKEWIQVDLGLLRFVTAVGTQGAISKET
E319K: FKCMEALGMESGEIHSDQITASSQYGTNWSVERSRLNYPENGWTPGKDSYKEWIQVDLGLLRFVTAVGTQGAISKET
C
WT Nrp1
empty vector
PAL-E Δ7
PAL-E Δ6
PAL-E Δ5
S346A, E348K T349A
S346A, E348K
E319K,D320K
E319K
AP-SEMA3A
AP-VEGF
NRP1

Figure 1.

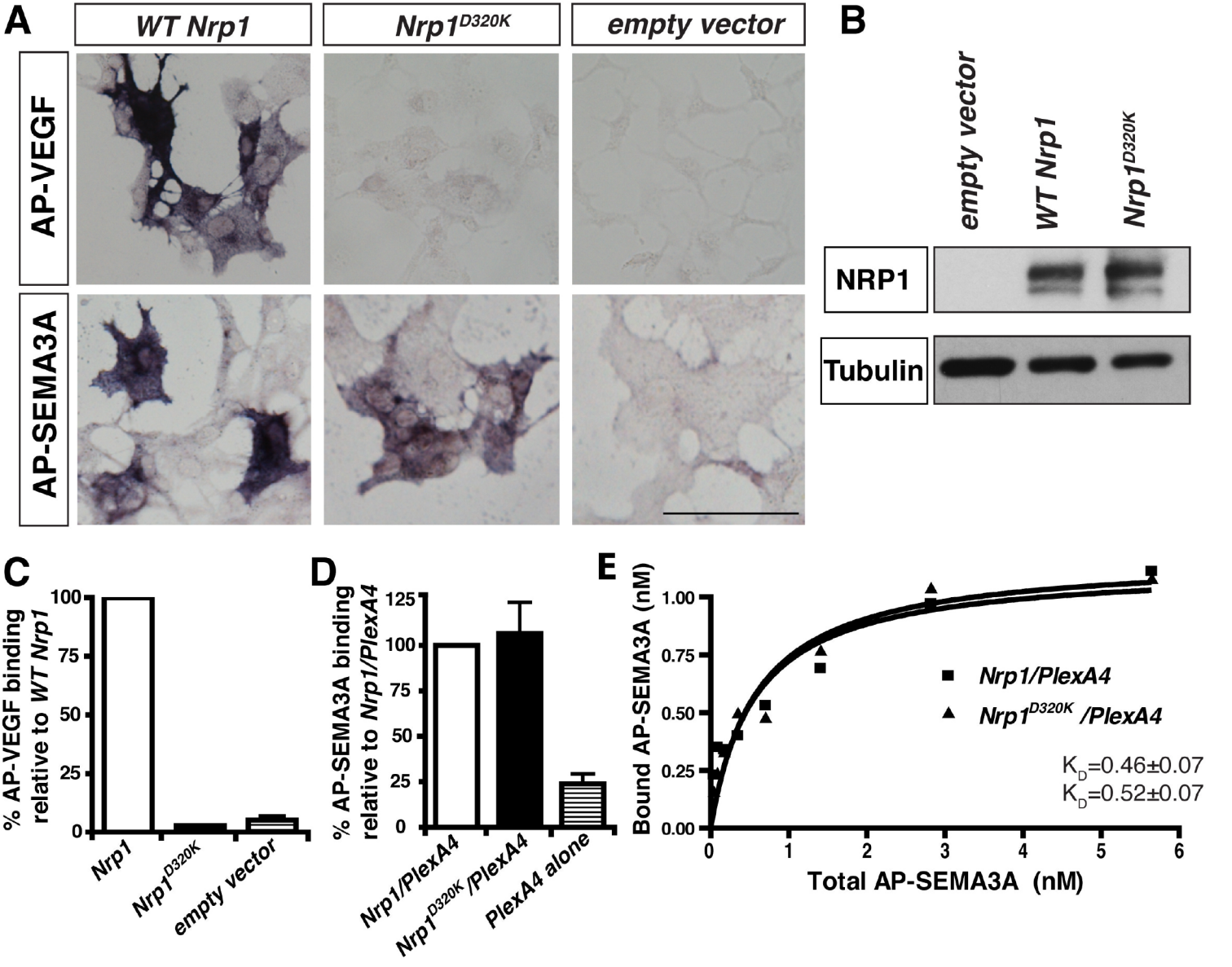
A
WT Nrp1
Nrp1D320K
empty vector
AP-VEGF
AP-SEMA3A
B
empty vector
WT Nrp1
Nrp1D320K
NRP1
Tubulin
C
% AP-VEGF binding relative to WT Nrp1
100
75
50
25
0
Nrp1
Nrp1D320K
empty vector
D
% AP-SEMA3A binding relative to Nrp1/PlexA4
125
100
75
50
25
0
Nrp1/PlexA4
Nrp1D320K /PlexA4
PlexA4 alone
E
Bound AP-SEMA3A (nM)
1.00
0.75
0.50
0.25
0.00
0
1
2
3
4
5
6
Total AP-SEMA3A (nM)
Nrp1/PlexA4
Nrp1D320K /PlexA4
KD=0.46±0.07
KD=0.52±0.07

Figure 2.

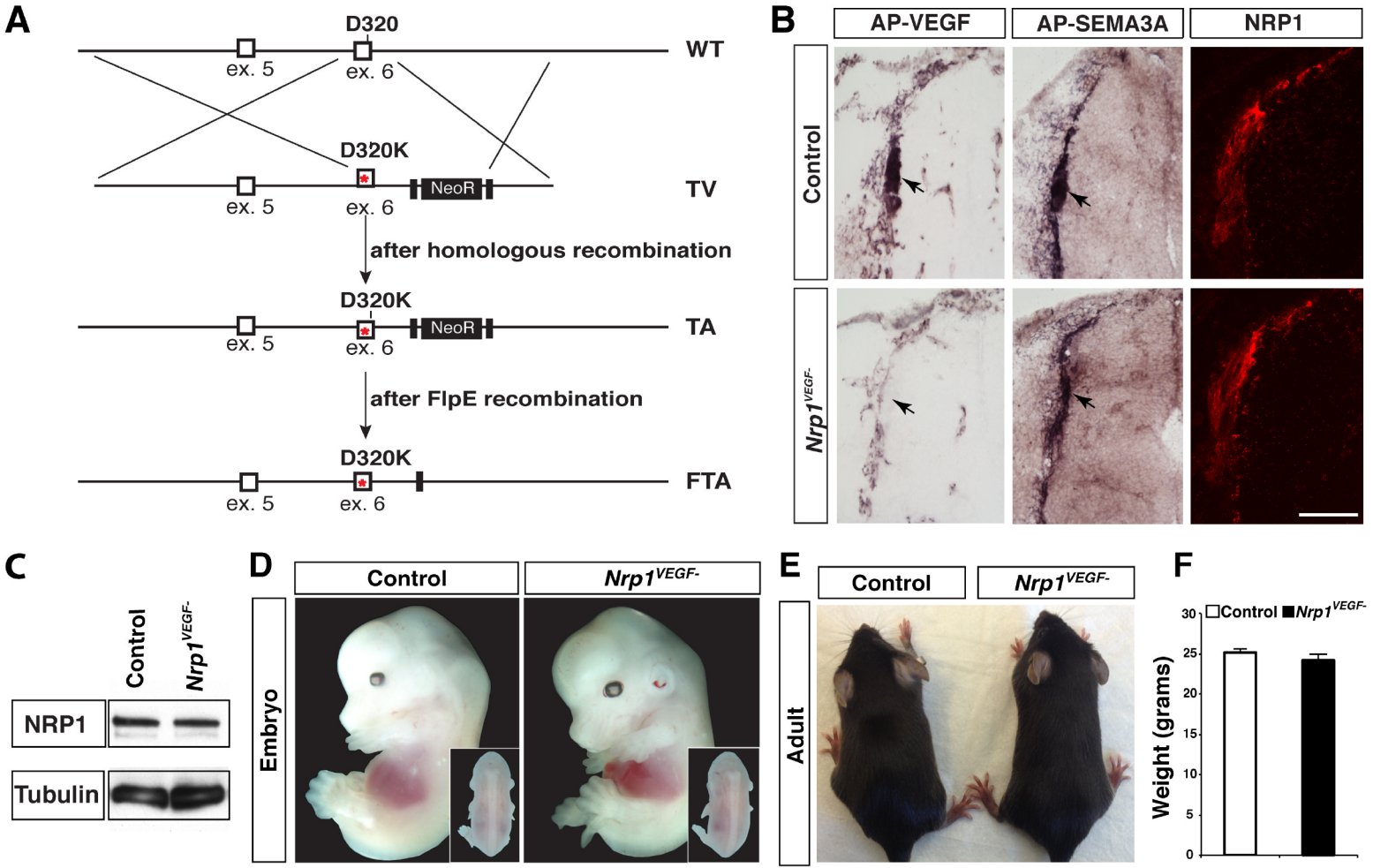
A
D320
ex. 5
ex. 6
WT
D320K
NeoR
TV
after homologous recombination
TA
after FlpE recombination
FTA
B
AP-VEGF
AP-SEMA3A
NRP1
Control
Nrp1VEGF-
C
Control
Nrp1VEGF-
NRP1
Tubulin
D
Control
Nrp1VEGF-
Embryo
E
Control
Nrp1VEGF-
Adult
F
Control
Nrp1VEGF-
Weight (grams)
30
25
20
15
10
5
0

Figure 3.

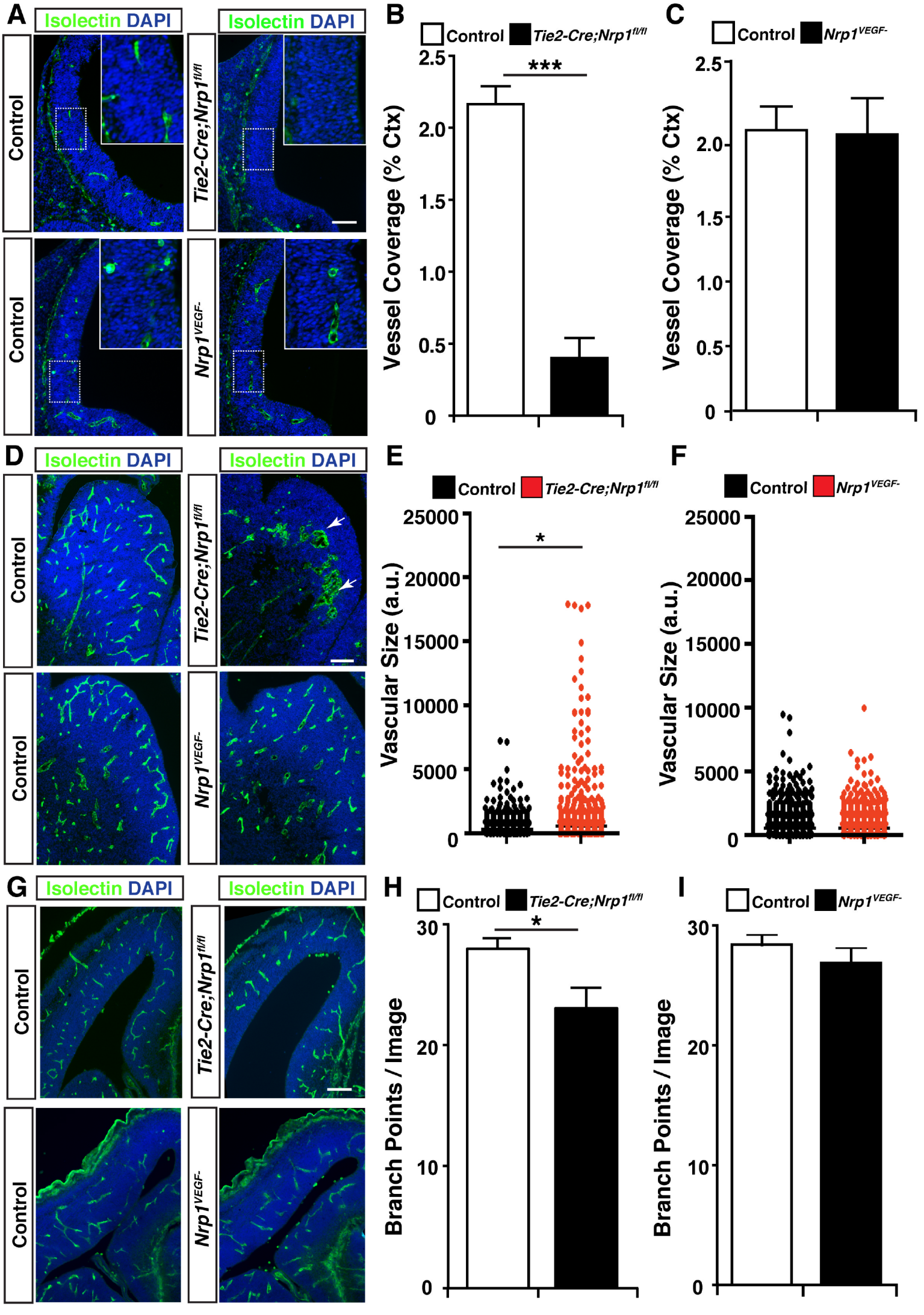
A
Isolectin DAPI
Isolectin DAPI
Control
Tie2-Cre;Nrp1fl/fl
Control
Nrp1VEGF-
B
Control
Tie2-Cre;Nrp1fl/fl
***
Vessel Coverage (% Ctx)
2.5
2.0
1.5
1.0
0.5
0
C
Control
Nrp1VEGF-
Vessel Coverage (% Ctx)
2.5
2.0
1.5
1.0
0.5
0
D
Isolectin DAPI
Isolectin DAPI
Control
Tie2-Cre;Nrp1fl/fl
Control
Nrp1VEGF-
E
Control
Tie2-Cre;Nrp1fl/fl
*
Vascular Size (a.u.)
25000
20000
15000
10000
5000
0
F
Control
Nrp1VEGF-
Vascular Size (a.u.)
25000
20000
15000
10000
5000
0
G
Isolectin DAPI
Isolectin DAPI
Control
Tie2-Cre;Nrp1fl/fl
Control
Nrp1VEGF-
H
Control
Tie2-Cre;Nrp1fl/fl
*
Branch Points / Image
30
20
10
0
I
Control
Nrp1VEGF-
Branch Points / Image
30
20
10
0

Figure 4.

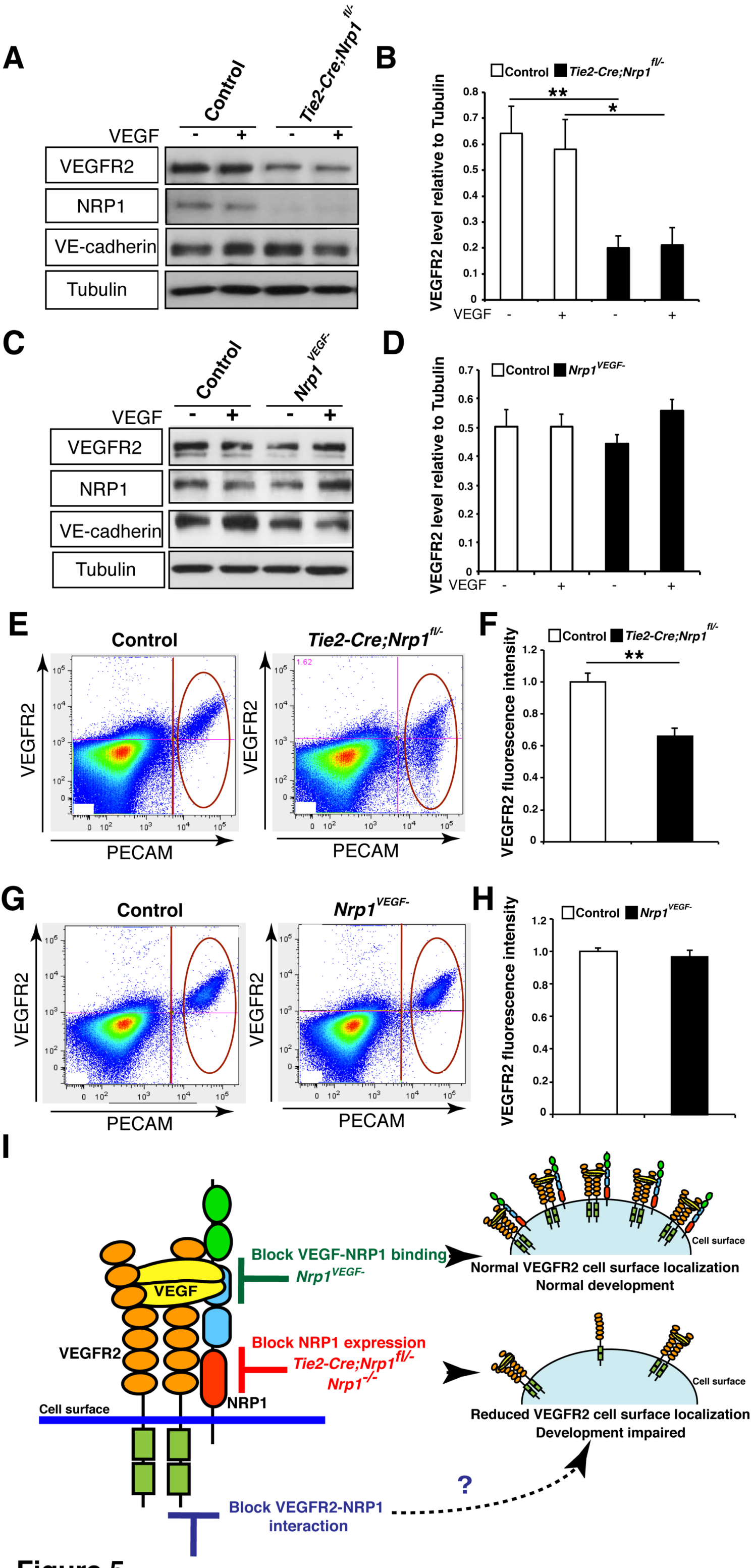
A
Control
Tie2-Cre;Nrp1fl/-
VEGF
- + - +
VEGFR2
NRP1
VE-cadherin
Tubulin
B
Control
Tie2-Cre;Nrp1fl/-
VEGFR2 level relative to Tubulin
0.8
0.7
0.6
0.5
0.4
0.3
0.2
0.1
0
**
*
VEGF - + - +
C
Control
Nrp1VEGF-
VEGF
- + - +
VEGFR2
NRP1
VE-cadherin
Tubulin
D
Control
Nrp1VEGF-
VEGFR2 level relative to Tubulin
0.7
0.6
0.5
0.4
0.3
0.2
0.1
0
VEGF - + - +
E
Control
Tie2-Cre;Nrp1fl/-
VEGFR2
PECAM
1.62
F
Control
Tie2-Cre;Nrp1fl/-
VEGFR2 fluorescence intensity
1.2
1.0
0.8
0.6
0.4
0.2
0
**
G
Control
Nrp1VEGF-
VEGFR2
PECAM
H
Control
Nrp1VEGF-
VEGFR2 fluorescence intensity
1.2
1.0
0.8
0.6
0.4
0.2
0
I
VEGF
VEGFR2
NRP1
Cell surface
Block VEGF-NRP1 binding
Nrp1VEGF-
Block NRP1 expression
Tie2-Cre;Nrp1fl/-
Nrp1-/-
Block VEGFR2-NRP1 interaction
?
Cell surface
Normal VEGFR2 cell surface localization
Normal development
Cell surface
Reduced VEGFR2 cell surface localization
Development impaired

Figure 5.

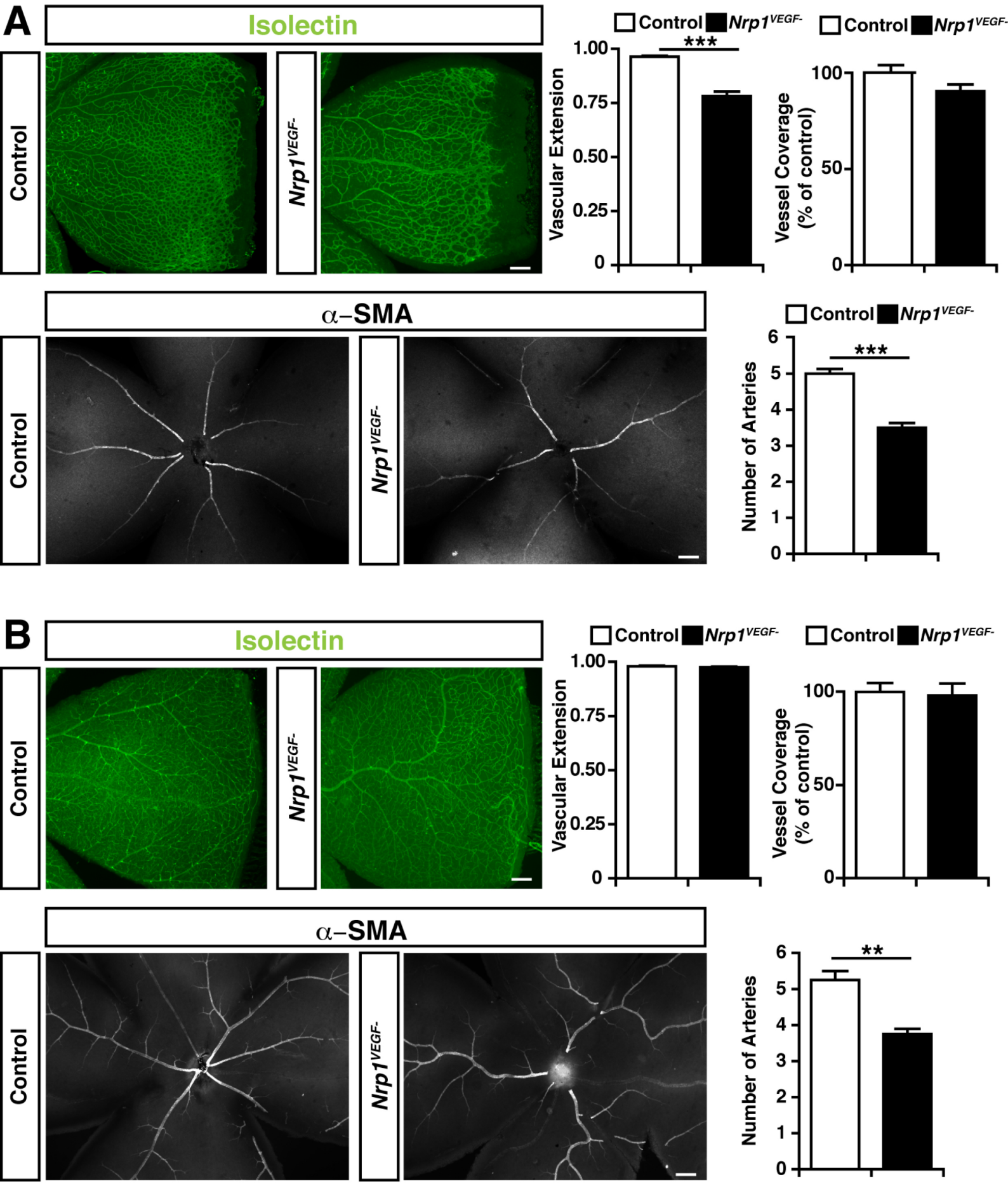
A
Isolectin
Control
Nrp1VEGF-
Control
Nrp1VEGF-
***
Vascular Extension
1.00
0.75
0.50
0.25
0
Control
Nrp1VEGF-
Vessel Coverage
(% of control)
100
50
0
α–SMA
Control
Nrp1VEGF-
Control
Nrp1VEGF-
***
Number of Arteries
6
5
4
3
2
1
0
B
Isolectin
Control
Nrp1VEGF-
Control
Nrp1VEGF-
Vascular Extension
1.00
0.75
0.50
0.25
0
Control
Nrp1VEGF-
Vessel Coverage
(% of control)
100
50
0
α–SMA
Control
Nrp1VEGF-
Control
Nrp1VEGF-
**
Number of Arteries
6
5
4
3
2
1
0

Figure 6.